

Dilaton-Axion Inflation with PBHs and GWs

Renata Kallosh and Andrei Linde

*Stanford Institute for Theoretical Physics and Department of Physics,
Stanford University, Stanford, CA 94305, USA*

E-mail: kallosh@stanford.edu, alinde@stanford.edu

ABSTRACT: We discuss two-stage dilaton-axion inflation models [1] and describe α -attractor models with either exponential or polynomial approach to the plateau. We implement one of the models of primordial black hole production proposed in [2] in the α -attractor context, and develop its supergravity version. The predictions of this model following from its polynomial attractor properties are: n_s and r are α -independent, r depends on the mass parameter μ defining the approach to the plateau. The tachyonic instability at the transition point between the two stages of inflation is proportional to the negative curvature of the hyperbolic space $\mathcal{R}_K = -2/3\alpha$. Therefore the masses of primordial black holes (PBHs) and the frequencies of small-scale gravitational waves (GWs) in this model show significant dependence on α .

Contents

1	Introduction	1
2	2-moduli inflationary models in hyperbolic geometry	4
2.1	From exponential to polynomial α -attractors	4
2.2	Hyperbolic geometry in half-plane coordinates	6
2.3	Supergravity version of the 2-moduli models	7
2.4	Dilaton-axion models in manifestly geometric variables	7
3	Observational predictions of the axion-dilaton attractor	9
3.1	CMB predictions for n_s and r	9
3.2	PBHs and GWs dependence on hyperbolic space curvature	10
4	Discussion	14
A	From half-plane to Poincaré disk coordinates	15

1 Introduction

Cosmological α -attractors represent a broad class of models which can describe all presently available inflation-related observational data by a choice of a single parameter (or a single combination of two parameters) [3–6]. These models can be formulated as models of a single real inflaton field φ . However, a particularly good theoretical motivation of these models is found in the framework of hyperbolic geometry based on $SL(2, \mathbb{R})$ symmetry or $SU(1, 1)$ symmetry of the kinetic terms. They arise naturally in supergravity where the scalar field is complex. These models were called attractors because their cosmological predictions are rather stable with respect to considerable modifications of their potential. Many of these predictions are determined by the underlying hyperbolic geometry.

There are two simplest classes of such models: T-models, with potentials $V \sim \tanh^2(\varphi/\sqrt{6\alpha})$, and E-models, with $V \sim (1 - e^{-\sqrt{2/3\alpha}\varphi})^2$, which predict $n_s = 1 - 2/N_e$ [3]. In addition, there is a class of polynomial attractors [5], which include KKLTI models with $V \sim \frac{\phi^2}{\phi^2+m^2}$ with $n_s = 1 - 3/2N_e$ and $V \sim \frac{\phi^4}{\phi^4+m^4}$ with $n_s = 1 - 5/3N_e$ [7, 8]. As one can see in Fig. 1, predictions of these simple single field inflation models completely cover the area favored by the latest Planck/BICEP/Keck data [9]. These models can describe any small value of r , all the way down to $r = 0$.

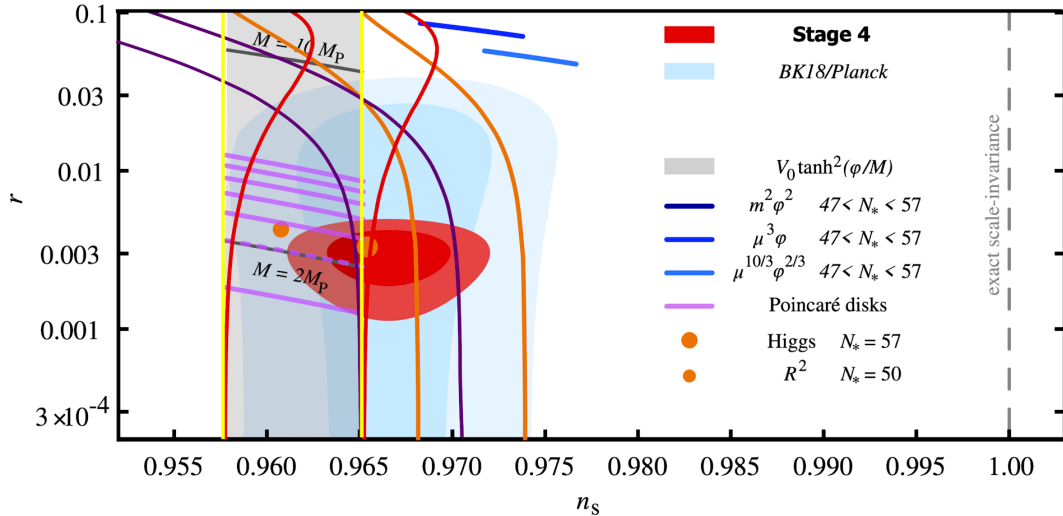


Figure 1: We use Figure 2 for the $n_s - r$ plane from ‘Snowmass2021 Cosmic Frontier: CMB Measurements White Paper’ [10]. Predictions of the simplest α -tractor T-models with $V \sim \tanh^2(\varphi/M)$ are shown in [10] as a grey band. Seven light purple lines show predictions of advanced α -tractor models inspired by string theory/M-theory models with 7 Poincaré disks. We added here also predictions of simplest E-models (area between two red lines), and predictions of quartic and quadratic polynomial KKLTI α -tractors (area between the dark purple and orange lines, respectively).

Historically, in most of the models of this type, one of the two components of the complex field was stabilized during inflation, and the remaining one played the role of the inflaton. In $SL(2, \mathbb{R})$ models the complex scalar is a dilaton-axion, the axion was usually stabilized, the dilaton was an inflaton. In $SU(1, 1)$ models the complex scalar represents a Poincaré disk with its radial and angular components. The angular component was stabilized, and the radial one played the role of the inflaton.

More recently it was realized that models where both of the components of the complex scalar field contribute to the two-field dynamics of inflation may have some potentially interesting features. The supergravity versions of such models were developed in [11–13] and in [1, 14]. It was shown, in particular, that it is possible to find supergravity description of models with arbitrary scalar potentials $V(T, \bar{T})$ [1, 12, 13]. Bosonic versions of two-stage inflation in hyperbolic geometry, mostly in disk variables, were studied in particular in [15–21]; more references can be found in [14].

The relation between the dilaton-axion type half-flat space metric and Poincaré disk metric describing hyperbolic geometry was discussed in the context of the α -tractors in [11, 16, 19]. All of these represent negative space curvature manifolds with the Kähler curvature $\mathcal{R}_K = -2/3\alpha$. This was the way these models were introduced in [4] in supergravity with one chiral multiplet, i.e. one complex scalar¹. In Fig. 2 we show Escher’s pictures for the

¹The curvature of the hyperbolic geometry with 2 real fields is $\mathcal{R} = -4/3\alpha$.

hyperbolic space in disk coordinates and in half-plane coordinates, from [11]. In particular, in the context of α -attractors [3] the relation between the T-models and E-models is the relation between Poincaré disk and half-flat space geometry: the kinetic terms are related by the change of coordinates, however, the potentials are not.

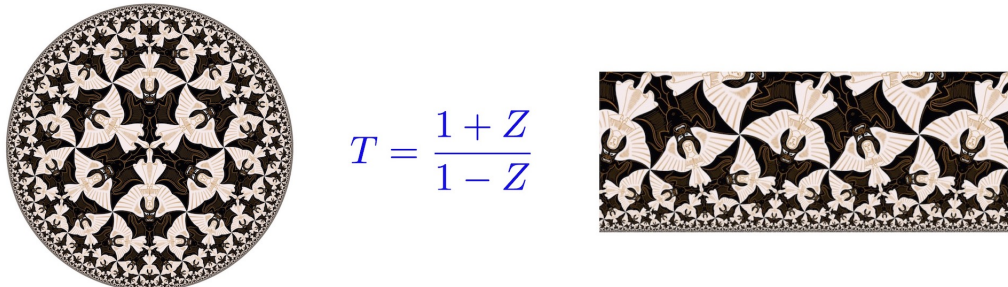


Figure 2: Here are Escher's pictures from [11] for the hyperbolic space in disk coordinates, $|Z|^2 < 1$, at the left and in half-plane coordinates, $T + \bar{T} > 0$, at the right. The boundary of the disk (with smaller and smaller angels and demons) is at $|Z| = 1$, the boundary of the half-flat space is (with smaller and smaller angels and demons) at $\text{Re } T = 0$.

Two-field inflationary models with non-trivial field metric have been used recently in the context of PBHs and GWs production. For single stage α -attractors, the potential with inflection point² was introduced and studied in [17, 19, 21] in disk coordinates. In two-stage hyperbolic geometry models, a far richer dynamical behavior is possible.

The new aspect of hyperbolic geometry, namely the metric in coordinates of the half-flat space taken in a standard stringy form of a dilaton-axion, appears to play an important role when the primordial black holes, gravitational waves production, and reheating are studied. Various cosmological models with PBHs and GWs production and stages of reheating/preheating were investigated recently both in disk and well as in half-plane coordinates. Some of these, such as [17–19, 21, 27, 28], were formulated in an obvious way as models in hyperbolic geometry, with curvature $\mathcal{R} = -4/3\alpha$, some others [2, 20] were not.

We will discuss here dilaton-axion inflationary models in hyperbolic geometry with exponential or polynomial α -attractors and their supergravity realization. We will show that one of the phenomenologically interesting dilaton-axion inflationary models proposed in [2] can be interpreted as a model with hyperbolic geometry. Then, using the methods developed in [1, 11–13], we will develop the supergravity generalization of this model.

This will allow us to use the α -attractor predictions for n_s and r and compare them with the numerical results obtained in [2]. We will find a very good agreement. Moreover, our new understanding of inflation in [2] will explain why the PBH masses and the frequencies of the GWs in this model depend on the curvature of the hyperbolic geometry.

²Importance of the inflection point near the exit of inflation for PBH's production was realized in [22–26].

2 2-moduli inflationary models in hyperbolic geometry

2.1 From exponential to polynomial α -attractors

In the simple case the one-inflaton T- and E-models [3] with *exponential approach to the plateau* have n_s and r independent of the properties of the large class of potentials. However, r depends on the curvature of the Kähler geometry $\mathcal{R}_K = -\frac{2}{3\alpha}$. At large values of φ the potential is $V_0(1 - e^{-\varphi/\mu} + \dots)$. The tensor to scalar ratio r depends on the parameter $\mu = \sqrt{3\alpha/2}$ describing the approach of the canonical field to the plateau.

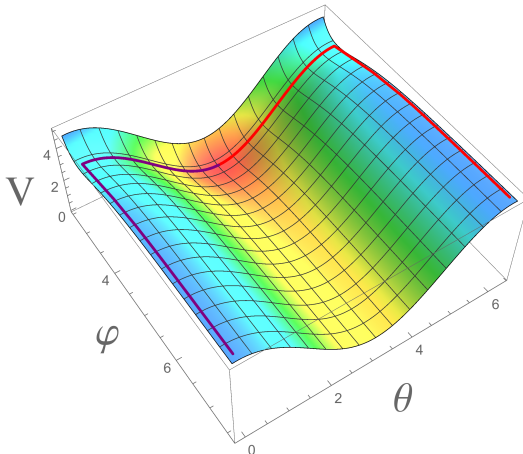


Figure 3: One of the two-stage dilaton-axion inflation models studied in [1]. The dilaton plateau potential stage starts with some initial value of the axion and dilaton fields. Two different trajectories (purple and red) correspond to two different initial values of the axion field. The axion during the dilaton inflation remains at its initial value, and starts moving only when the field ϕ approaches its minimum at $\phi = \phi_0$. Notice the sharp turn of the inflationary trajectories at $\phi = \phi_0$.

In *polynomial approach to the plateau* one-inflaton α -attractor models [5] the potential at large values of φ is $V_0(1 - (\frac{\mu}{\varphi})^k + \dots)$. In these models n_s depends on k , whereas r depends both on k and μ , [7, 8]. Both n_s and r do not depend on the curvature of the Kähler geometry $\mathcal{R}_K = -\frac{2}{3\alpha}$.

Here we will describe the two-stage dilaton-axion models of inflation developed in [1], as well as their their generalizations. The original E-model dilaton potential with the exponential approach to plateau studied in [1] can be replaced by a polynomial attractor [5], i.e. we can replace an E-model potential by the one which has a power law approach to the plateau, a quadratic KKTTI attractor [7, 8].

Both types of models have the same dilaton-axion kinetic term

$$\mathcal{L}_{\text{kin}} = \frac{1}{2} \left[(\partial\varphi)^2 + e^{2\sqrt{\frac{2}{3\alpha}}\varphi} (\partial a)^2 \right]. \quad (2.1)$$

The potentials studied in [1] are

$$V(\varphi, a) = V_0 \left(1 - e^{-\sqrt{\frac{2}{3\alpha}}(\varphi - \varphi_0)} \right)^2 + \frac{1}{2} m_a^2 a^2 . \quad (2.2)$$

The dilaton potential in (2.2) is the E-model exponential α -attractor with the position of the minimum at $\varphi = \varphi_0$. The axion has a mass term potential³.

We now replace the potential $V_0 \left(1 - e^{-\sqrt{\frac{2}{3\alpha}}(\varphi - \varphi_0)} \right)^2$ with an exponential approach to the plateau used in [1] by a polynomial attractor [5], which has a power law approach to the plateau, and find the dilaton-axion potential of the form

$$V(\varphi, a) = V_0 \frac{\varphi^2}{\varphi^2 + \mu^2} + \frac{1}{2} m_a^2 a^2 . \quad (2.3)$$

In a class of models considered in [2, 20], where the PBHs can be produced, a kinetic term was chosen in the form

$$\mathcal{L}_{\text{kin}} = \frac{1}{2} [\partial_\mu \varphi \partial^\mu \varphi + f(\varphi) \partial_\mu a \partial^\mu a] . \quad (2.4)$$

One of the models studied in [2] has

$$f(\phi) = e^{2b_1 \varphi} , \quad (2.5)$$

but it was not clear whether this choice may have a fundamental geometric interpretation, and whether it is any better than another choice $f(\phi) = e^{2b_2 \varphi^2}$ also studied in [2].

Now we can relate it to the hyperbolic geometry of α -attractors and incorporate this model in supergravity with the corresponding Kähler geometry iff

$$f(\phi) = e^{2b_1 \varphi} = e^{2\sqrt{\frac{2}{3\alpha}} \varphi} , \quad \text{i.e.} \quad b_1 = \sqrt{\frac{2}{3\alpha}} . \quad (2.6)$$

Thus, if we choose the kinetic term in [2] as in (2.5), we can relate their parameter b_1 to the Kähler curvature,

$$b_1^2 = -\mathcal{R}_K = \frac{2}{3\alpha} , \quad e^{2b_1 \varphi} = e^{2\sqrt{|\mathcal{R}_K|} \varphi} . \quad (2.7)$$

The phenomenology of this cosmological model introduced in [2], which we now embedded into hyperbolic geometry, was studied extensively with regard to PBHs and GWs. We will describe the microscopic origin of both models in (2.2), and in (2.3) in supergravity, and extract an interesting information about phenomenology from the fact that the model in (2.3)

³The axion potential used in [1] at $\phi = \phi_0$ is more general, it is proportional to $\cos^2 \frac{\theta}{2}$ where $\theta - \pi = \sqrt{\frac{2}{3\alpha}} a$. For small deviation of the axion from the minimum the model becomes the one shown in (2.2).

is a dilaton-axion inflationary model in hyperbolic geometry which has attractor properties of polynomial α -attractors.

Importantly, one of the parameters in this model defining the properties of PBHs and GWs is actually a curvature of the hyperbolic geometry, as shown in (2.6). Other features of this model following from the fact that it is embedded into hyperbolic geometry with inflationary plateau potential approaching polynomially [5] will be identified. We will show that n_s and r are defined by their plateau potential attractor values [5, 7].

The point of transition to the second stage of inflation is characterized by the effective mass square of the isocurvature perturbations m_{eff}^2 . It can abruptly and temporarily become large and negative; we will find out that $m_{\text{eff}}^2 \sim \mathcal{R}_K$.

2.2 Hyperbolic geometry in half-plane coordinates

A simple way to introduce this class of metrics is to start with equation (5) in [29], where the Kähler potential defining the Kähler geometry metric is given by

$$K = -3\alpha \ln(T + \bar{T}), \quad (2.8)$$

in notation ($c = 3\alpha$) adapted to the definition of α -attractor E-models. The Kähler metric is $g_{T\bar{T}} = \partial_T \partial_{\bar{T}} K$ and the geometry defines the kinetic term for a complex scalar

$$\mathcal{L}_{\text{kin}} = 3\alpha \frac{\partial_\mu T \partial_\nu \bar{T} g^{\mu\nu}}{(T + \bar{T})^2}. \quad (2.9)$$

It has an $SL(2, \mathbb{R})$ symmetry. It was explained around equations (5) and (6) in [29] that the case $3\alpha = 3$ corresponds to the dilaton-axion in string theory [30] where the total volume is defined by the dilaton, and no-scale supergravity [31, 32]. The case $3\alpha = 1$ is a single dilaton-axion case. Now we know more examples of discrete $3\alpha = 7, 6, 5, 4, 3, 2, 1$ [33] as well as continuous 3α in the context of $\mathcal{N} = 1$ supergravity [3, 4]. Following [29] we present our complex field T , a half-plane coordinate of the hyperbolic geometry, as a dilaton and an axion:

$$T(x) = e^{-\sqrt{\frac{2}{3\alpha}}\varphi(x)} + i\sqrt{\frac{2}{3\alpha}} a(x), \quad T + \bar{T} > 0. \quad (2.10)$$

The real part of the T -field is an exponent of the dilaton φ , therefore clearly positive, which explains the ‘half-plane’ coordinate name. The dilaton-axion kinetic term (2.9) is

$$\mathcal{L}_{\text{kin}} = \frac{1}{2} \left[\partial_\mu \varphi \partial_\nu \varphi g^{\mu\nu} + e^{2\sqrt{\frac{2}{3\alpha}}\varphi} \partial_\mu a \partial_\nu a g^{\mu\nu} \right]. \quad (2.11)$$

Here φ is a dilaton and a is the axion whose kinetic term couples exponentially to the dilaton.

$$\varphi = -\sqrt{\frac{3\alpha}{2}} \ln \frac{1}{2}(\bar{T} + T), \quad a = \frac{1}{2i} \sqrt{\frac{3\alpha}{2}}(\bar{T} - T). \quad (2.12)$$

The total non-gravitational Lagrangian, including the potential, in geometric variables is

$$\mathcal{L} = 3\alpha \frac{\partial_\mu T \partial_\nu \bar{T} g^{\mu\nu}}{(T + \bar{T})^2} - V(T, \bar{T}). \quad (2.13)$$

2.3 Supergravity version of the 2-moduli models

The supergravity version of the hyperbolic geometry models with both dilaton and axion evolving during inflation was developed in [11–13] and [1]. In addition to the dilaton-axion multiplet T we need a nilpotent one, $X^2 = 0$. The Kähler potential and the superpotential for models of our interest here were proposed and studied in [13] and in [1].

We generalize supergravity models in [13] and in [1] by introducing two different parameters. One is describing the breaking of supersymmetry in the X directions, we call it F_X , the other describing the breaking of supersymmetry in the T directions will be W_0 as in [13] and in [1]. Our model is now defined as follows, for $\alpha < 1$

$$K = -3\alpha \ln(T + \bar{T}) + G_{X\bar{X}} X \bar{X}, \quad W = W_0 + F_X X. \quad (2.14)$$

$$G_{X\bar{X}} = \frac{F_X^2}{(T + \bar{T})^{3\alpha} V(T, \bar{T}) + 3W_0^2(1 - \alpha)}. \quad (2.15)$$

The value of the potential in this model, at $X = 0$ is

$$V_{\text{final}} = V(T, \bar{T}). \quad (2.16)$$

Thus, in terms of the dilaton and axion bosonic fields of our supergravity models (2.14), (2.15), the non-gravitational part of the action is

$$\mathcal{L}(\varphi, a) = \frac{1}{2} [(\partial\varphi)^2 + e^{2\sqrt{\frac{2}{3\alpha}}\varphi} (\partial a)^2] - V(T(\varphi, a), \bar{T}(\varphi, a)), \quad (\partial\varphi)^2 \equiv \partial_\mu \varphi \partial_\nu \varphi g^{\mu\nu}. \quad (2.17)$$

This expression is the same as the one in eq. (2.13), for any potential $V(T, \bar{T})$.

2.4 Dilaton-axion models in manifestly geometric variables

Now we can present these models in geometric hyperbolic variables T where the action is given in eq. (2.13) and T is defined in eq. (2.10). Using

$$\frac{1}{2}(\bar{T} + T) \equiv t, \quad \frac{1}{2i}\sqrt{\frac{3\alpha}{2}}(\bar{T} - T) \equiv a, \quad (2.18)$$

we can present the potentials of the models in [1, 2] which can be used for the supergravity version of the model.

The supergravity version of the Hypernatural inflation model (2.2) requires a potential depending on geometric fields T, \bar{T} . It is given by

$$V(T, \bar{T}) = V_0(1 - t)^2 + \frac{1}{2}m_a^2 a^2. \quad (2.19)$$

where $t(T, \bar{T})$ and $a(T, \bar{T})$ are given in eq. (2.18). Replacing t by the canonically normalized field φ results in (2.2) [1].

The cosmological model developed in [2] is

$$\mathcal{L} = \frac{1}{2} [-(\partial_t \phi)^2 - e^{2b_1 \phi} (\partial_t \chi)^2] - V_0 \frac{\phi^2}{\mu^2 + \phi^2} - \frac{1}{2} m_\chi^2 \chi^2. \quad (2.20)$$

It is now easy to recognize it as the one we presented in eqs. (2.1), (2.3) under condition

$$b_1 = \sqrt{\frac{2}{3\alpha}}, \quad \varphi \rightarrow \phi, \quad a \rightarrow \chi. \quad (2.21)$$

It can also be given in the form with the $SL(2, \mathbb{R})$ invariant metric (2.9). The potential breaks the $SL(2, \mathbb{R})$ symmetry of the kinetic term and is given by the expression where the inflaton part of the potential was presented in [5]. Namely, the potential of model [2] in geometric variables is

$$V(T, \bar{T}) = V_0 \frac{\ln^2 t}{c^2 + \ln^2 t} + \frac{1}{2} m_a^2 a^2, \quad c^2 = \mu^2 |\mathcal{R}_K|. \quad (2.22)$$

where $t(T, \bar{T})$ and $a(T, \bar{T})$ are given in eq. (2.18). This also means that the supergravity version of the model in [2] with (2.5) is now available in eqs. (2.14), (2.15), (2.16), (2.22). It is a dilaton-axion cosmological attractor model of the type described in [5].

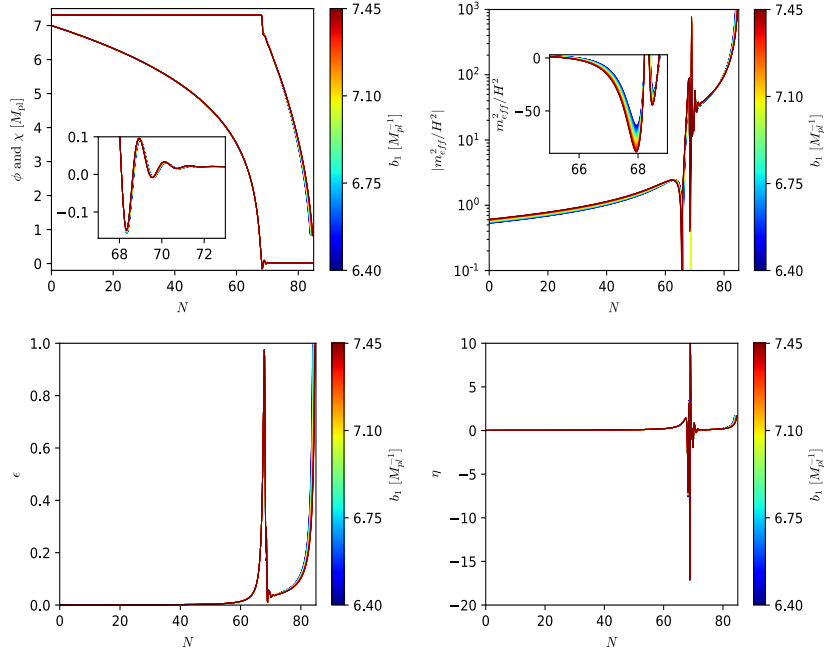


Figure 4: The cosmological predictions of a model in [2], Fig. 1 there based on numerical solution. The figures show the evolution of the dilaton and axion, of the slow-roll parameters and the effective mass of the isocurvature perturbation. The dependence on α , which here is the dependence on the color codifying $b_1 = \sqrt{\frac{2}{3\alpha}}$, is practically absent. This is in agreement with attractor eqs. (3.1).

3 Observational predictions of the axion-dilaton attractor

3.1 CMB predictions for n_s and r

The α -attractor models with stabilized axion have stable attractor predictions. In case of the polynomial α -attractors which we have here, we can first look at numerical examples studied in [2] and see if they are supported by the attractor values presented in eq. (2.14) in [5]. For slow roll parameters we have

$$n_s = 1 - \frac{3}{2N_e}, \quad r = \frac{\sqrt{2}\mu}{N_e^{3/2}}. \quad (3.1)$$

We compare this prediction with the numerical cases studied in [2] and displayed in their Fig. 1, we show them in our Fig. 4.

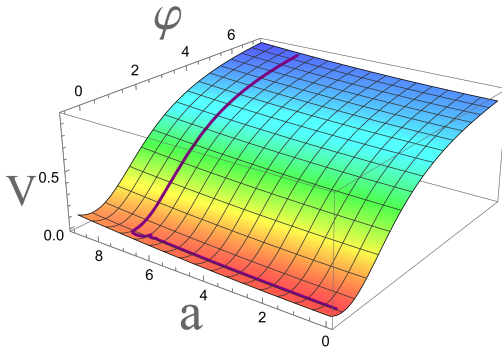


Figure 5: The dilaton-axion potential in terms of a dilaton which has a canonical kinetic term and the axion a which has an exponential coupling to dilaton in his kinetic term. Parameters are from [2]: $\mu = \sqrt{6}$, $\frac{V_0}{500} = m_a^2$, and we took $\alpha = 0.0136$ for $b_1 = 7$. The dilaton stage of inflation happens when the dilaton field rolls down the blue plateau of the KKLTI potential, The second stage is the axion chaotic inflation due to the quadratic potential shown as the red area.

We can explain the main features of the model based on its attractor properties as well as numerical solutions supporting them, see Figs. 4, 5. The effective mass of the axion is suppressed by the exponential factor $e^{-\sqrt{\frac{2}{3\alpha}}\varphi}$ due to kinetic term coupling. The axion is exponentially light at large φ at the plateau, and starts moving only when the field φ approaches the minimum of its potential at $\varphi = 0$, and the exponential suppression of its effective mass disappears. This is the ‘rolling on the ridge effect’ effect found in [1, 12]. Thus the dilaton stage of inflation ends at $a \approx a_i$. After φ reaches $\varphi = 0$, the axion in models with $a_i \neq 0$, undergoes a stage of chaotic inflation due to the axion potential $\frac{1}{2}m_a^2 a^2$. The number of e-folds at this stage depends on how far is a_i from its minimum $a = 0$ when it rolls along the valley with the quadratic potential shown as the elongated red area at $\varphi = 0$ in Fig. 5. We plot the trajectory of the fields during the two-stage inflation. At the turning point we found that ϵ jumps to 1 and η jumps down to -17 and rises up to $+10$ before settling to the slow roll axion inflation stage.

For the total number of e-folds to be 57, the number of e-foldings N_e responsible for observations in eq. (3.1) should be smaller than 57, in view of additional e-folds at the axion stage:

$$N_{\text{total}} = N_e + N_{\text{axion}} \approx 57 . \quad (3.2)$$

Note that if initially at $\phi = 7$ the axion would be placed at $a = 0$, in the middle of the plateau, it would be only one stage of inflation with $N_e = 57$, $n_s \approx 0.97$.

We will consider 4 different cases which differ by the choice of the initial position of the axion, as we see in Table 1 in [2] and reproduced here in Fig. 6.

	$\phi_i [M_{\text{pl}}]$	$\chi_i [M_{\text{pl}}]$	n_s	r
SKA	7.0	9.3	0.9184	0.042
LISA	7.0	7.31	0.9537	0.020
BBO	7.0	6.55	0.9601	0.017
ET	7.0	5.6	0.9640	0.014

Figure 6: Initial conditions for the dilaton and axion and n_s and r .

The number of e-foldings N_e which we have to use in our attractor formula (3.1) can be identified by the values of n_s or r in the table. We get N_e from r using the table, and calculate n_s with the same N_e we find a good agreement with the table of numerical solutions given in [2]. Namely, we find for SKA, LISA, BBO, ET examples from (3.1)

$$\begin{aligned}
 N_e = 19 \quad n_s = 0.921 \quad r = 0.042 \\
 N_e = 32 \quad n_s = 0.952 \quad r = 0.020 \\
 N_e = 35 \quad n_s = 0.957 \quad r = 0.017 \\
 N_e = 39 \quad n_s = 0.961 \quad r = 0.014
 \end{aligned} \quad (3.3)$$

One should take into account also that the parameters $\mu = \sqrt{6}$ and $r > 10^{-2}$ are above the values of these parameters where the attractor regime is reached in these models, as explained in [7]. One can also see it in Fig. 3 in [5], which shows that the attractor regime is reached only for $r \lesssim 10^{-2}$.

And we definitely see the trend which is also clear from the properties of the dilaton-axion model of inflation. In particular, the attractor values of n_s and r in eq. (3.1) are α -independent, which clearly explains why in Fig. 4 almost all curves for different values of $b_1 = \sqrt{\frac{2}{3\alpha}}$ coincide.

3.2 PBHs and GWs dependence on hyperbolic space curvature

Here in Fig. 7 we describe the transition area at the fixed value of Kähler curvature. The kinetic term for the axion field is $e^{2\sqrt{|\mathcal{R}_K|\varphi}}(\partial a)^2$. It means that the ‘physical distance’ is $e^{\sqrt{|\mathcal{R}_K|\varphi}}\partial a$, which is the reason why at large positive φ the axion field a is not moving for a long time. We can see it in Fig. 4 at the upper left corner where $\chi = a$ remains at his

initial position for a long time during the first stage of the dilaton inflation. When the field φ reached his minimum at $\varphi = 0$ this protection of the axion position at its initial value vanishes. Moreover, when φ becomes negative during the oscillation near the minimum, this factor becomes $e^{-\sqrt{|\mathcal{R}_K||\varphi|}\partial a}$. This forces the axion first to change dramatically from its initial position and after a while a slow roll axion inflation takes place.

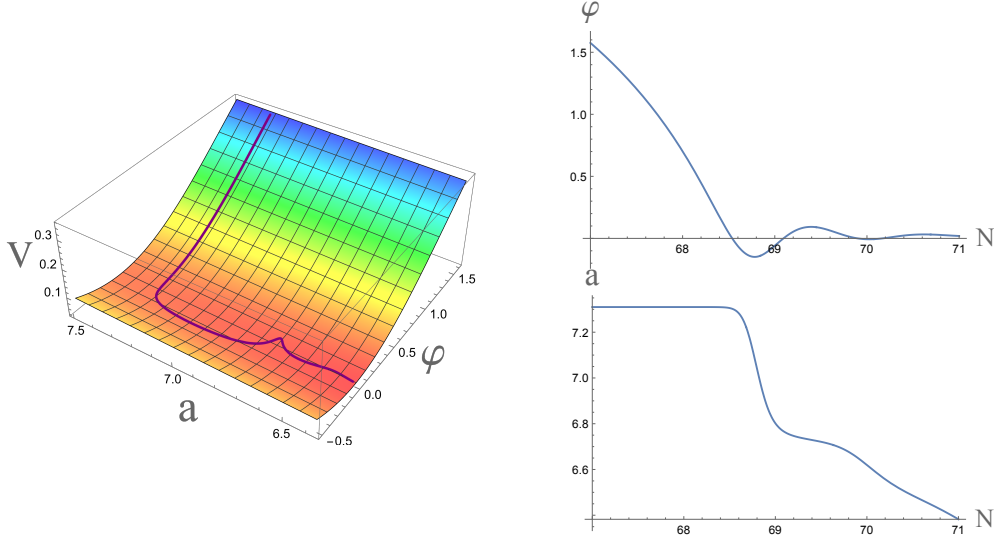


Figure 7: Near transition area where the axion inflation stage replaces the dilaton inflation. We can see the correlation between the fast change of the axion and φ crossing zero and oscillating to negative value.

Note that this effect is significant for large curvatures $|\mathcal{R}_K|$ and less significant for smaller ones, which explains the color dependence of the value of m_{eff}^2/H^2 in the blow-up region in the upper right plot in Fig. 4. The color there is codifying $b_1 = \sqrt{\frac{2}{3\alpha}}$, it changes from blue to red when b_1 is increasing. Note that in all figures in in Fig. 4 there is no color dependence. The only exception is a blow-up region in the upper right plot of the effective mass of isocurvature perturbations m_{eff}^2/H^2 . This color-dependence of m_{eff}^2/H^2 is practically absent during the first and the second stage of inflation, it is only present at the point of transition. Our Fig. 7 compliments a blow-up region in the upper right plot of the effective mass of isocurvature perturbations m_{eff}^2/H^2 in Fig. 4. The effective mass of isocurvature perturbations m_{eff}^2 becomes temporarily negative at the transition between the two stages of inflation and leads to a transient tachyonic amplification of the isocurvature perturbations leading to a large peak in the power spectrum. We found an additional explanation of the color dependence of m_{eff}^2 defined in [2] at the region of transition where $\phi_{\text{tran}} \approx 0$. We have found that the effective mass to Hubble ratio depends on the Kähler curvature $\mathcal{R}_K = -b_1^2$ as follows

$$\frac{m_{\text{eff}}^2}{H^2} \Rightarrow 5 \mathcal{R}_K \left(\frac{\partial a}{\partial N} \right)^2 + \dots \quad (3.4)$$

The ... in (3.4) are for terms which mildly depend on \mathcal{R}_K , only in the form $e^{\sqrt{|\mathcal{R}_K|}\phi_{tran}}$ with $\phi_{tran} \approx 0$, or are independent on \mathcal{R}_K .

The first term is linear in Kähler curvature, depends on how fast the axion a changes as a function of N , and it is dominant at the transition, the second term depends on Kähler curvature times $\phi_{tran} \approx 0$. This means that at the region of transition the negativity of the effective isocurvature mass is due to the negativity of the Kähler curvature as the first term in eq. (3.4) shows.

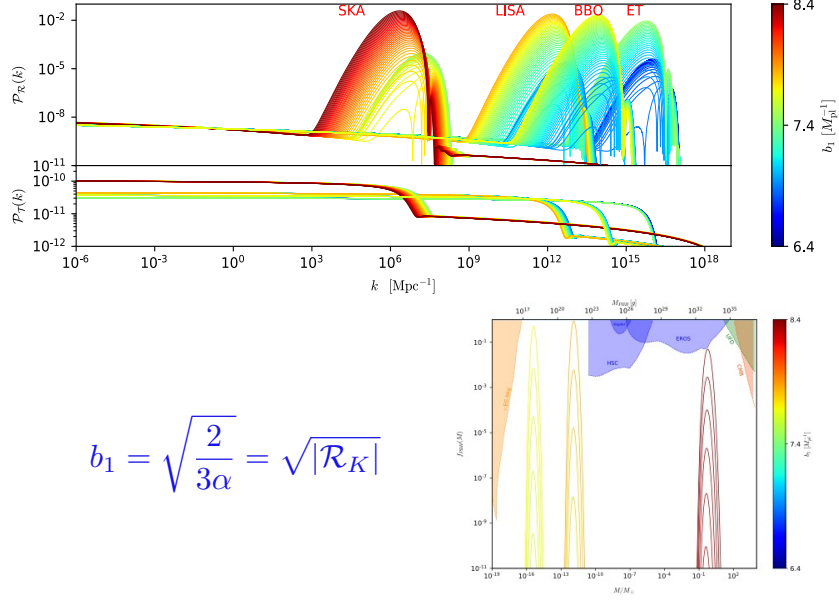


Figure 8: The cosmological predictions of a model in [2] where the potential with polynomial approach to plateau is embedded into hyperbolic geometry has α -dependent predictions for the the tensor power spectra at the end of inflation and for the properties of the PBHs.

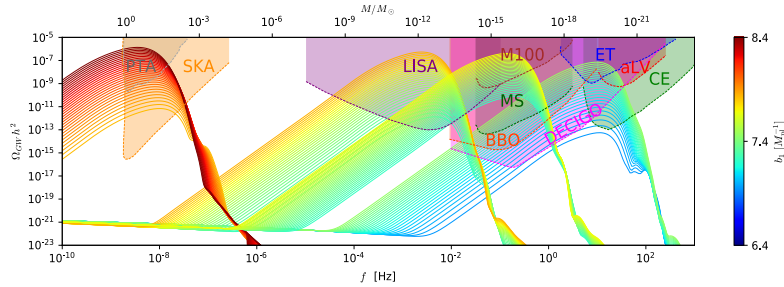


Figure 9: The cosmological predictions of a model in [2] where b_1 -dependence of the properties of the induced GW is presented by color coding and $b_1 = \sqrt{\frac{2}{3\alpha}}$.

The upper right plot in Fig. 4 shows that the most negative effective mass of isocurvature

perturbations in the blow-up region can be explained by the formula (3.4) which says that for bigger $|\mathcal{R}_K|$ the most negative value is reached (the red part of the figure at $N \approx 68$). This property of the ratio m_{eff}^2/H^2 explains why the phenomenology of the PBHs and GWs strongly depends on the curvature. In Figs. 8 and 9 we reproduce figures from [2] where one can see that the change in $b_1 = \sqrt{\frac{2}{3\alpha}}$ leads to dramatic changes in phenomenology. In particular, when $6.4 \leq b_1 \leq 8.4$ we need very small α so that $0.028 \leq 3\alpha \leq 0.049$ and very high Kähler curvature $-\mathcal{R}_K = b_1^2 \gtrsim 40$.

An additional set of models with parameters $\frac{V_0}{m_a^2} = R = 30, 1050, 3800$ was also studied in [2], see Figure 10 here.

	$\chi_i [M_{\text{pl}}]$	$V_0 [10^{-10} M_{\text{pl}}^4]$	R	$b_1 [M_{\text{pl}}]^{-1}$
1	3.2	6.4	30	9.466
2	7.31	7.08	500	7.837
3	8.1	7.6	1050	7.382
4	8.5	8.21	3800	6.233

Figure 10: Changes in axion masses $m_a^2 = \frac{V_0}{R}$ and initial conditions for the axion and the resulting change in Kähler curvature $b_1^2 = \frac{2}{3\alpha} = -\mathcal{R}_K$.

It was observed in [14] that rapid-turn inflation models in hyperbolic geometry tend to have high-curvature. This underscores the difficulty of obtaining such models from string theory. For example, the ones associated with M-theory and type IIB string theory in [34] without rapid terms have $3\alpha = 7, 6, 5, 4, 3, 2, 1$.

Interestingly, with increasing $R = \frac{V_0}{m_a^2}$ which corresponds to lighter axions, the required value of b_1 is decreased and α is increased. We can provide here a qualitative explanation of this feature, comparing the cases with $R = 500$ and $R = 3800$ in [2].

The mass squared of the axion is decreasing from the case described in details with $m_a^2 = \frac{V_0}{R}$ to the case \tilde{m}_a^2 with different V_0 and R and (case 2 and case 4 in Fig. 10). Also the initial conditions change from a_i to \tilde{a}_i . We can compare the effective mass of the axion in case 2 and case 4

$$e^{-2b_1\phi} m_a^2 a_i^2, \quad e^{-2\tilde{b}_1\tilde{\phi}} \tilde{m}_a^2 \tilde{a}_i^2. \quad (3.5)$$

It follows that

$$e^{2b_1\phi_c - \ln C^2} \approx e^{2\tilde{b}_1\tilde{\phi}_c}. \quad (3.6)$$

and numerically $\ln C^2 \approx 1.57$. If we assume that we can compare these two models at the point $\phi_c \approx 0.49$ which is approximately the same in both cases, we find that

$$b_1 - \tilde{b}_1 \approx 1.55, \quad (3.7)$$

to be compared with the difference between $b_1 = 7.837$ to $\tilde{b}_1 = 6.233$, which is 1.6.

This is desirable modification of the parameters in the model since increasing α would be a step towards smaller Kähler curvature. For example, with $3\alpha = 1$ the Kähler curvature is

$-\mathcal{R}_K = 2/3\alpha = 2$. This is a smallest Poincaré disk associated with string theory. Smaller α are possible in $\mathcal{N} = 1$ supergravity but the ones like $3\alpha = 1, 2, 3, 4, 5, 6, 7$ originate from string theory and maximal $\mathcal{N} = 8$ supergravity.

It would be also interesting if the models with smaller values of μ can be investigated, so that the system gets closer to the attractor regime and maybe works for smaller Kähler curvature.

4 Discussion

All presently existing inflation-related data can be described by simple single-field inflationary models with one parameter [5, 6]. Moreover, the simple α -attractor models with $3\alpha = 7, 6, 5, 4, 3, 2, 1$ form the set of discrete B-mode targets, see Fig. 2 in [35], where these 7 Poincaré disks are shown as some of the main targets for LiteBIRD. We present the predictions of the single stage inflationary α -attractors in Fig. 1.

Exponential α -attractors make the nearly universal predictions $n_s = 1 - 2/N_e$ and $r = 12\alpha/N_e^2$. Using these expressions one can derive a useful expression for the curvature of the Kähler geometry $\mathcal{R}_K = -\frac{2}{3\alpha}$:

$$\mathcal{R}_K = -\frac{2(1 - n_s)^2}{r}. \quad (4.1)$$

Thus by measuring n_s and r one can find the curvature \mathcal{R}_K .

For polynomial attractors [5] this simple relation is no longer valid. Nevertheless, in this paper we argued that one can obtain interesting information about the curvature of the Kähler geometry \mathcal{R}_K by investigation of formation of PBHs and small-scale GWs.

For single field exponential α -attractors with an inflection point, this possibility was studied in [17, 19, 21]. The current conclusion is that the PBHs produced in such models are light, $M_{\text{PBH}} < 10^8$ g, due to the fact that the effective number of e-folds in such models is smaller than the one in models without the inflection point, and n_s cannot be smaller than the lowest value established by Planck [19]. The peak of the GW signal is constrained to be at very high frequencies.

In this paper we studied the models developed in [1] and replaced there the exponential α -attractor part of these modes by a polynomial quadratic α -attractor, which predicts a greater value of $n_s = 1 - \frac{3}{2N_e}$ [5]. If there is a second stage of inflation driven by the axion field, it makes N_e in the attractor equation for n_s smaller. The value of n_s decreases, but if the second stage of inflation is not too long, n_s decreases from its greater value $n_s = 1 - \frac{3}{2N_e}$ but still remains within the Planck bounds on n_s . This tends to remove the upper bound on the mass of PBHs of the type $M_{\text{PBH}} < 10^8$ g which was found in [19].

One of the most interesting and phenomenologically successful models of the PBHs production was proposed in [2], but its fundamental interpretation was not clear. We implemented this

model in the context of polynomial α -attractors, and developed its supergravity version. This embedding suggests a microscopic origin of the parameters used in this model. In particular, the parameter b_1 in the axion kinetic term $e^{2b_1\phi}(\partial\chi)^2$ of [2] depends on the curvature of the Kähler geometry, $b_1^2 = -\mathcal{R}_K = \frac{2}{3\alpha}$.

The predictions of this model following from its polynomial attractor properties are: n_s and r are α -independent, whereas r depends on the mass parameter μ defining the approach of the inflationary potential to the plateau. We confirmed that the CMB predictions of this model are consistent with the attractor formula (3.1) for the polynomial α -attractor model. We also explained a significant dependence of the PBH masses and GW frequencies on hyperbolic geometry curvature: the effective tachyonic mass of isocurvature perturbations depends linearly on \mathcal{R}_K at the point of transition from the dilaton to axion stage of inflation, as shown in eq. (3.4).

This suggests that by finding the spectrum of masses of PBHs and the frequencies of the GWs, in combination with measuring n_s, r one may find information about the curvature of the Kähler geometry \mathcal{R}_K in this class of models.

Acknowledgement

We are grateful to Y. Yamada for useful comments on this work, and to A. Achúcarro, D.-G. Wang, Y. Welling and Y. Yamada for the collaboration on the earlier projects which led to this paper. We are grateful to M. Sasaki and A. Starobinsky for the stimulating talks on inflation and PBHs production at the February 2022 Kyoto conference ‘Gravity - The Next Generation’. This work is supported by SITP and by the US National Science Foundation Grant PHY-2014215.

A From half-plane to Poincaré disk coordinates

To describe two-stage inflationary models based on hyperbolic geometry it is important to make a choice of geometric variables which are most convenient for understanding the cosmological evolution. In this paper we used the half-plane coordinates $T + \bar{T} > 0$ with the complex field T defining the dilaton-axion pair (φ, a)

$$T(x) = e^{-\sqrt{\frac{2}{3\alpha}}\varphi(x)} + i\sqrt{\frac{2}{3\alpha}} a(x). \quad (\text{A.1})$$

Alternatively, one could use the Poincaré disk coordinates $Z = re^{i\theta} = \frac{T-1}{T+1}$.

The map between the polar coordinates of the disk (r, θ) and planar coordinates of the hyperbolic field space (φ, a) is presented in [19] with $\varphi = u, a = v$.

$$\varphi(r, \theta) = \sqrt{\frac{3\alpha}{2}} \ln \left[\frac{1 + r^2 + 2r \cos \theta}{1 - r^2} \right], \quad a(r, \theta) = 2\sqrt{\frac{3\alpha}{2}} \left[\frac{r \sin \theta}{1 + r^2 + 2r \cos \theta} \right] \quad (\text{A.2})$$

The relevant kinetic term in (r, θ) variables is

$$-\frac{3\alpha}{(1-r^2)^2}[(\partial r)^2 + r^2(\partial\theta)^2] = -\frac{1}{2}(\partial\sigma)^2 - \frac{3\alpha}{4}\sinh^2\left(\sqrt{\frac{2}{3\alpha}}\sigma\right)(\partial\theta)^2 \quad (\text{A.3})$$

The dilaton-axion potential which we use is given in eq. (2.3). We have shown it in Fig. 5 together with the inflationary trajectory. To find the expression for this potential in polar coordinates, one should put expressions for $\varphi(r, \theta)$ and $a(r, \theta)$ in (A.2) into the potential (2.3), and then replace the geometric variable r by the canonically normalized field σ such that $r = \tanh\sqrt{\frac{2}{3\alpha}}\sigma$, $0 \leq \sigma < \infty$.

We present the plot of the potential $V(\sigma, \theta)$ for $\alpha = O(1)$ in Fig. 11.

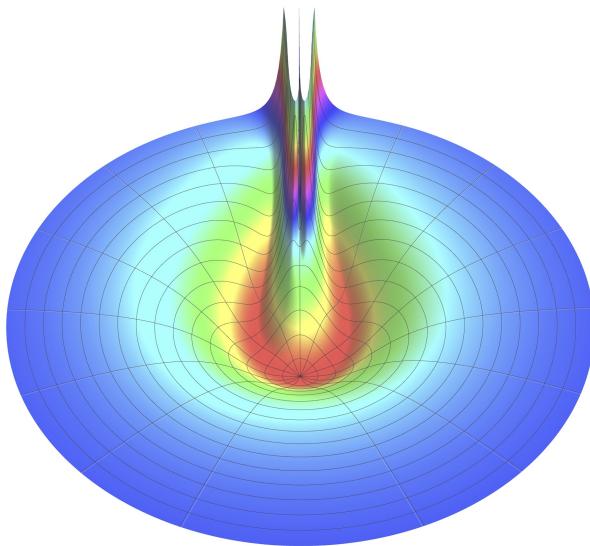


Figure 11: The potential $V(\sigma, \theta)$. For the purpose of visualization we use $\alpha = 1$ case in this plot. For much smaller values of α the ridges become very narrow. The red area at the lower part of the potentials corresponds to $\varphi \approx 0$.

With some effort, one can figure out the behavior of the inflationary trajectory in (σ, θ) coordinates in Fig. 11. In particular, the straight chaotic inflation valley at $\varphi \approx 0$ shown as a red area in Fig. 5 corresponds to the strongly curved red valleys in Fig. 11. This bending makes the description of the last stage of inflation slightly more complicated. For smaller values of α , such as $\alpha \sim 10^{-2}$ used in [2], it is hard to draw and interpret figures like Fig. 11, because the ridges and the red valleys shown in these figures become extremely thin.

The potential is singular at $r \rightarrow 1$, $\theta \rightarrow \pi$ [19]. The reason is that the axion field (A.2) becomes infinitely large in this limit, and the chaotic inflation potential $\frac{1}{2}m_a^2 a^2$ diverges in this limit $a \rightarrow \infty$. This is the standard feature of monomial chaotic inflation potentials. This singularity disappears if one replaces $\frac{1}{2}m_a^2 a^2$ by a periodic axion potential as in [1, 12].

Thus, it is possible to change coordinates in the moduli space by a Cayley transform, $T = \frac{1+Z}{1-Z}$, $Z = \frac{T-1}{T+1}$, as shown in Figs. 2, 5, 11. It is amazing that we can map the behavior of the axion potential in the infinite range $-\infty < a < +\infty$ to the vicinity of the disc boundary. However, the cosmological two-stage inflation models, which we study in this paper, look much simpler in the dilaton-axion form (2.10), (2.17) and in Fig. 5.

References

- [1] A. Linde, D.-G. Wang, Y. Welling, Y. Yamada and A. Achúcarro, *Hypernatural inflation*, *JCAP* **1807** (2018) 035 [[1803.09911](#)].
- [2] M. Braglia, D.K. Hazra, F. Finelli, G.F. Smoot, L. Sriramkumar and A.A. Starobinsky, *Generating PBHs and small-scale GWs in two-field models of inflation*, *JCAP* **08** (2020) 001 [[2005.02895](#)].
- [3] R. Kallosh, A. Linde and D. Roest, *Superconformal Inflationary α -Attractors*, *JHEP* **11** (2013) 198 [[1311.0472](#)].
- [4] S. Ferrara, R. Kallosh, A. Linde and M. Porrati, *Minimal Supergravity Models of Inflation*, *Phys. Rev.* **D88** (2013) 085038 [[1307.7696](#)].
- [5] R. Kallosh and A. Linde, *Polynomial α -attractors*, [2202.06492](#).
- [6] R. Kallosh and A. Linde, *BICEP/Keck and cosmological attractors*, *JCAP* **12** (2021) 008 [[2110.10902](#)].
- [7] R. Kallosh, A. Linde and Y. Yamada, *Planck 2018 and Brane Inflation Revisited*, *JHEP* **01** (2019) 008 [[1811.01023](#)].
- [8] J. Martin, C. Ringeval and V. Vennin, *Encyclopædia Inflationaris*, *Phys. Dark Univ.* **5-6** (2014) 75 [[1303.3787](#)].
- [9] BICEP/KECK collaboration, *Improved Constraints on Primordial Gravitational Waves using Planck, WMAP, and BICEP/Keck Observations through the 2018 Observing Season*, *Phys. Rev. Lett.* **127** (2021) 151301 [[2110.00483](#)].
- [10] C.L. Chang et al., *Snowmass2021 Cosmic Frontier: Cosmic Microwave Background Measurements White Paper*, in *2022 Snowmass Summer Study*, 3, 2022 [[2203.07638](#)].
- [11] R. Kallosh and A. Linde, *Escher in the Sky*, *Comptes Rendus Physique* **16** (2015) 914 [[1503.06785](#)].
- [12] A. Achúcarro, R. Kallosh, A. Linde, D.-G. Wang and Y. Welling, *Universality of multi-field α -attractors*, *JCAP* **1804** (2018) 028 [[1711.09478](#)].
- [13] Y. Yamada, *$U(1)$ symmetric α -attractors*, *JHEP* **04** (2018) 006 [[1802.04848](#)].
- [14] V. Aragam, R. Chiovoloni, S. Paban, R. Rosati and I. Zavala, *Rapid-turn inflation in supergravity is rare and tachyonic*, [2110.05516](#).
- [15] P. Christodoulidis, D. Roest and E.I. Sfakianakis, *Angular inflation in multi-field α -attractors*, *JCAP* **11** (2019) 002 [[1803.09841](#)].
- [16] S. Garcia-Saenz, S. Renaux-Petel and J. Ronayne, *Primordial fluctuations and non-Gaussianities in sidetracked inflation*, *JCAP* **07** (2018) 057 [[1804.11279](#)].

- [17] I. Dalianis, A. Kehagias and G. Tringas, *Primordial black holes from α -attractors*, *JCAP* **01** (2019) 037 [[1805.09483](#)].
- [18] L. Anguelova, *On Primordial Black Holes from Rapid Turns in Two-field Models*, *JCAP* **06** (2021) 004 [[2012.03705](#)].
- [19] L. Iacconi, H. Assadullahi, M. Fasiello and D. Wands, *Revisiting small-scale fluctuations in α -attractor models of inflation*, [2112.05092](#).
- [20] S. Pi and M. Sasaki, *Primordial Black Hole Formation in Non-Minimal Curvaton Scenario*, [2112.12680](#).
- [21] I. Dalianis and G.P. Kodaxis, *Reheating in runaway inflation models via the evaporation of mini primordial black holes*, [2112.15576](#).
- [22] J. Garcia-Bellido, A.D. Linde and D. Wands, *Density perturbations and black hole formation in hybrid inflation*, *Phys. Rev. D* **54** (1996) 6040 [[astro-ph/9605094](#)].
- [23] J. Garcia-Bellido and E. Ruiz Morales, *Primordial black holes from single field models of inflation*, *Phys. Dark Univ.* **18** (2017) 47 [[1702.03901](#)].
- [24] J.M. Ezquiaga, J. Garcia-Bellido and E. Ruiz Morales, *Primordial Black Hole production in Critical Higgs Inflation*, *Phys. Lett. B* **776** (2018) 345 [[1705.04861](#)].
- [25] C. Germani and T. Prokopec, *On primordial black holes from an inflection point*, *Phys. Dark Univ.* **18** (2017) 6 [[1706.04226](#)].
- [26] G. Ballesteros and M. Taoso, *Primordial black hole dark matter from single field inflation*, *Phys. Rev. D* **97** (2018) 023501 [[1709.05565](#)].
- [27] O. Iarygina, E.I. Sfakianakis, D.-G. Wang and A. Achúcarro, *Universality and scaling in multi-field α -attractor preheating*, *JCAP* **06** (2019) 027 [[1810.02804](#)].
- [28] O. Iarygina, E.I. Sfakianakis, D.-G. Wang and A. Achúcarro, *Multi-field inflation and preheating in asymmetric α -attractors*, [2005.00528](#).
- [29] R. Kallosh, *On inflation in string theory*, *Lect. Notes Phys.* **738** (2008) 119 [[hep-th/0702059](#)].
- [30] S. Kachru, R. Kallosh, A.D. Linde and S.P. Trivedi, *De Sitter vacua in string theory*, *Phys. Rev. D* **68** (2003) 046005 [[hep-th/0301240](#)].
- [31] E. Cremmer, S. Ferrara, C. Kounnas and D.V. Nanopoulos, *Naturally Vanishing Cosmological Constant in $N=1$ Supergravity*, *Phys. Lett. B* **133** (1983) 61.
- [32] J.R. Ellis, A.B. Lahanas, D.V. Nanopoulos and K. Tamvakis, *No-Scale Supersymmetric Standard Model*, *Phys. Lett. B* **134** (1984) 429.
- [33] S. Ferrara and R. Kallosh, *Seven-disk manifold, α -attractors, and B modes*, *Phys. Rev. D* **94** (2016) 126015 [[1610.04163](#)].
- [34] R. Kallosh, A. Linde, T. Wrase and Y. Yamada, *IIB String Theory and Sequestered Inflation*, *Fortsch. Phys.* **69** (2021) 2100127 [[2108.08492](#)].
- [35] LITEBIRD collaboration, *Probing Cosmic Inflation with the LiteBIRD Cosmic Microwave Background Polarization Survey*, [2202.02773](#).